Influence of slit asymmetry on blow-off and flashback in methane/hydrogen laminar premixed burners

Hugo Pers, Pierre-Alexandre Masset, Enrique Flores-Montoya, Laurent Selle, Thierry Schuller

Influence of slit asymmetry on blow-off and flashback in methane/hydrogen laminar premixed burners

H. Pers[a,b], P.A. Masset[a,c], E. Flores-Montoya[a], L. Selle[a], T. Schuller[a,d]

[a]*Institut de Mécanique des Fluides de Toulouse, IMFT, Université de Toulouse, CNRS, Toulouse, France*
[b]*Hydrogen Research and Development Laboratory, SERMETA, France*
[c]*LE2H - Commissariat à l'Energie Atomique, CEA Saclay, France*
[d]*Institut universitaire de France (IUF)*

Abstract

One way to decarbonize the heat production sector is to gradually replace natural gas with hydrogen. The design of laminar premixed burners capable of operating with both methane and hydrogen is however challenging as these fuels have drastically different burning properties, which narrows the operating range. While methane flames face limitations in stabilization due to blow-off at high power, hydrogen flames tend to be susceptible to flashback at low power. This study investigates the effects of slits symmetry breaking on the blow-off of methane flames and flashback of hydrogen flames through two-dimensional direct numerical simulations of canonical asymmetrical slit configurations, revealing uneven interactions between the main openings and smaller auxiliary slits. The equations governing the reactive flow dynamics are coupled to a heat transfer solver in the solid phase to elucidate the thermal and hydrodynamic mechanisms determining the operability limits. Viscous dissipation in the small auxiliary slits together with a substantial preheating of the fresh gases by heat redistribution through the solid phase is found to govern flame stabilization in asymmetrical geometries, improving blow-off resistance of methane/air flames. Then, flashback of hydrogen/air flame is found to be driven by the competition between (i) the mass flow rate distribution between the main and auxiliary slits, (ii) preheating of the gas through the auxiliary slits and (iii) the ability of the main and auxiliary slits to quench the flame. The interplay of these phenomena gives rise to complex behaviors, wherein asymmetrical configurations could exhibit significantly enhanced resistance to flashback compared to symmetrical geometries. This conclusion, verified for different burner thicknesses and slit spacing, may be used to guide the design of fuel-flexible laminar burners.

Keywords:
FUEL FLEXIBILITY, PERFORATED PLATE, HYDROGEN SUBSTITUTION, DOMESTIC BURNER, ASYMMETRY, FLAME-WALL INTERACTION
2023 MSC: 00-01, 99-00

Novelty and significance statement

1. Analyzing the effect of slits symmetry breaking on blow-off of methane flames and flashback of hydrogen flames for multi-perforated laminar burners.
2. Defining a strategy for wall heat flux redistribution to assess the asymmetrical interaction between the main and auxiliary flames through the flame-holder.
3. Demonstrating and explaining the positive impact of symmetry breaking on the blow-off resistance of methane flames.
4. Highlighting the substantial and non-monotonous impact of symmetry breaking on hydrogen flame flashback.
5. Identifying the interplay of thermal and hydrodynamic mechanisms in asymmetrical slits leading to improvement of flashback resistance for hydrogen/air flames compared to symmetrical configurations.

Author contributions

H.P.: designed and performed research, analyzed data, wrote paper. P-A.M.: designed research, reviewed and corrected paper. E.F-M.: supported data processing, reviewed and corrected paper. L.S.: designed research, reviewed and corrected paper. T.S.: designed research, reviewed and corrected paper.

1. Introduction

Hydrogen is a promising fuel for the decarbonization of domestic and industrial heating appliances [1, 2], and of particular interest within power-to-gas strategies [3, 4]. However, the conversion of natural-gas burners to hydrogen is fundamentally challenging [5, 6, 7]. One of the main issues is the high laminar burning velocity, S_L^0, of hydrogen-air mixtures, which is roughly four times larger than for natural-gas-air mixtures at constant adiabatic flame temperature. An immediate consequence is that premixed hydrogen burners are

more prone to flashback, raising major safety concerns [8]. This issue is rooted in the small quenching distance [9] that allows hydrogen-enriched flames to propagate through narrow channels and to stabilize closer to the burner walls. These two features cause operational difficulties in multi-perforated burners used in most domestic and industrial laminar boilers.

The higher burner temperature and subsequent preheating of the reactants promotes flashback [10, 11, 12] and limits the potential hybridization rate of existing end-use systems to a maximum of about 20% H_2 in volume [2, 13], which only represents 7% in terms of CO_2 abatement. The transition from hydrocarbons to hydrogen therefore requires the development of fuel-flexible burners, capable of handling both natural gas and hydrogen over the largest possible power range. To avoid flashback at low power, the burner geometry can be adjusted to increase the inlet bulk velocity of reactants so as to maintain the kinematic balance between the flow and the flame front propagation. This approach is satisfying for hydrogen flames, which can resist blow-off at very high inlet velocities thanks to a broader flammability range and to preferential diffusion effects [14, 15, 16]. However this strategy increases the risk of blow-off for natural gas at high power [17, 18, 19, 20].

Extending the lean blow-off limit is indeed a design guideline for many premixed laminar burners due to the relatively low burning velocity of laminar premixed flames powered by hydrocarbon fuels [21]. As such, the design of hydrogen-flexible burners must comply with conflicting requirements: (i) ensure resistance to lean blow-off of slow methane flames at high power and (ii) avoid flashback of fast hydrogen flames at the lower end of the power range. Mechanisms governing these two limits are briefly reviewed.

The seminal work of Lewis and Von Elbe [22, 23] considers blow-off to occur when a certain Critical Velocity Gradient (CVG) is reached at the exit of the flame-holder. While extending the flame stretch theory of Karlovitz [24], it however neglects the effect of flame curvature on the stretch. This theory was since challenged numerous times [25, 26, 27]. These studies concluded that using an area-increase factor provided better blow-off predictions than the Karlovitz theory for inverted flames. The role of heat transfer in stabilization of such flames was also discussed at length [27, 28, 29].

Kedia et al. [18] argued that these results could not be extended to configurations corresponding to multi-perforated plates, and described conditions leading to lean blow-off for methane-air flames stabilized over such devices. Blow-off was found to be triggered when the gradient of the flame base displacement speed normal to the flame becomes lower than the gradient of the flow velocity along the same direction. Prior to blow-off, increasing the inlet velocity was also associated with a decrease in the radius of curvature at the flame anchoring point until reaching an asymptotic value, comparable to the flame thickness. The role of heat losses to the burner was found to be critical. In parallel, flame-holders such as perforated plates or bluff-body were demonstrated to greatly improve the blow-off resistance of premixed flames [30, 31]. The main mechanisms leading to this improvement were identified as heat and flow recirculation in the wake of solid components of the burner [14, 15, 32], and proven to greatly depend on the geometry of the bluff-body [33, 34, 35]. These recent studies confirm what was previously observed experimentally: adding a ring smaller than the rim to a Bunsen-type burner greatly improves flame stabilization and its resistance to blow-off, by anchoring an auxiliary flame that surrounds the main conical flame [36, 37].

The Critical Velocity Gradient (CVG) framework proposed by Lewis and Von Elbe [22, 38] also yields conditions leading to flashback of laminar premixed flames stabilized above circular holes and slits. It has since been applied to numerous configurations [39, 40] and tested for various fuel mixtures, flame-holder geometries [41, 42] and inlet gas temperatures [43, 44]. The original CVG model however overlooks several mechanisms relevant for flame stabilization. The inclusion of flame stretch effects [34] and preferential diffusion [45, 46] was shown to be necessary to correctly predict flashback limits of lean hydrogen laminar premixed flames characterized by negative Markstein lengths [34, 47, 48, 49].

Another limitation of the original CVG model is the lack of heat exchange between the flame and the wall. Already mentioned in the original study as a strong shortcoming of the CVG model, heat exchange between solid and gaseous phases has been shown to be critical in many burners with small holes [11, 32, 50, 51, 52, 53]. Recent experiments also highlighted the role of the thermal state of the burner and the inability of the CVG model to predict flashback at very high wall temperatures [11, 54]. In extreme cases, it was shown that the high reactivity and short ignition delay of hydrogen-air preheated mixtures [55] led to flashback induced by autoignition inside the burner itself, a mechanism totally different from CVG [54]. This emphasizes the importance of both hydrodynamic and thermal management during the design of a hydrogen burner.

It is clear that the geometry of the burner alters the conditions leading to flashback and blow-off and the relative importance of the different phenomena discussed in the previous paragraphs, the objective being to identify an optimal geometry delaying both flashback and blow-off. The influence of the geometry of perforated burners has already been explored for both methane [10, 19, 56] and hydrogen [34]. Attention was given on slit size, slit spacing and wall thickness. Notably, it was shown that a larger distance between the slits could, to a certain extent, increase the wall temperature due to an increased contact surface area between the wall and the recirculating burnt gases. Conversely, it was proven that increasing the plate thickness contributes to decrease the wall temperature.

From a fundamental perspective, no study has yet considered the case of asymmetrical slit configurations as presented in Fig. 1, either for methane blow-off or for hydrogen flashback. The combination of main slits or holes separated by smaller auxiliary slits is indeed a technology used in domestic boilers

to improve methane flame resistance to blow-off (see for example [54]).

A two-dimensional numerical analysis is conducted in order to elucidate the impact of slits symmetry breaking on the blow-off and flashback dynamics of methane-air and hydrogen-air flames. The simulations take into account conjugated heat transfer, aiming at identifying the thermal and hydrodynamic mechanisms that support or impede the burner fuel flexibility in symmetrical and asymmetrical configurations. The study is organized as follows. Section 2 presents the numerical setup. Section 3 elaborates the heat flux analysis that has been carried out to separate the respective roles of the main slit and of the auxiliary slit. Section 4 explores the mechanisms driving blow-off resistance of asymmetrical methane flames. Section 5 describes the effects of asymmetry on flashback of hydrogen flames. The conclusions drawn emphasize the importance of considering slits asymmetry to improve the flexibility of multi-perforated laminar premixed burners with respect to methane/hydrogen mixtures.

2. Numerical setup

Two fuels are considered : methane, as a surrogate for natural gas and hydrogen. Their properties at the inlet temperature $T_u = 300\,\mathrm{K}$ are computed using Cantera with the GRIMECH 3.0 mechanism, and are summarized in Tab. 1. For methane, the equivalence ratio $\phi = 0.785$ is fixed within the operating range of domestic boiler burners. In order to accommodate industrial needs regarding thermal load on structures, it is chosen to keep the same adiabatic flame temperature $T_{ad} = 1974\,\mathrm{K}$ for the hydrogen-air mixture as for the methane-air flame and hence to lower the equivalence ratio to $\phi = 0.676$ for hydrogen. This strategy leads to different laminar burning velocities S_L^0 and thermal flame thicknesses δ_f (Tab. 1). The laminar burning velocity of the hydrogen mixture is four times the laminar burning velocity of the methane mixture and the hydrogen flame thickness is reduced by about 40% with respect to the methane flame. These two mixtures correspond to the most stringent constraints on flashback and blow-off for the chosen hybridization strategy. Though 2D and stationnary, these simulations are labeled Direct Numerical Simulations (DNS) because all the flow and flame scales of the laminar flows considered are resolved. Moreover, the chemical kinetics is fairly detailed so that the computational framework is the same as what is classically labeled as DNS, i.e. the simulation of fully resolved 3D turbulent flows.

Table 1: Equivalence ratio ϕ, adiabatic flame temperature T_{ad}, laminar burning velocity S_L^0 and flame thickness $\delta_f = (T_b - T_u)/\max(\nabla T)$ for an inlet temperature $T_u = 300\,\mathrm{K}$ and ambient pressure $p = 1$ atm.

Fuel	ϕ	T_{ad} [K]	S_L^0 [m/s]	δ_f [mm]
CH_4	0.785	1974	0.26	0.54
H_2	0.676	1973	1.14	0.34

2.1. Governing equations and code coupling

Coupled fluid/solid simulations are performed using the codes AVBP and AVTP developed by CERFACS [57, 58]. AVBP is a fully-compressible explicit code solving the reactive Navier-Stokes equations in the gas phase, and is used here with the Lax-Wendroff convective scheme of second-order accuracy in time and space [59]. Chemical kinetics of both methane and hydrogen are solved using an Analytically Reduced Chemistry (ARC) scheme developed and validated in [60], comprising 15 transported species, 9 species under the quasi-steady-state approximation and 138 reversible reactions. Ideal gas law is assumed and gravity is neglected. Species diffusion is computed using the classical Hirschfelder and Curtiss approximation. The Prandtl number is assumed to remain constant Pr=0.701, as well as species Lewis numbers Le_k. AVTP is a heat transfer solver for solids, that uses the same second order Galerkin diffusion scheme for spatial discretization as AVBP, and a time integration based on a first-order forward Euler scheme [61].

AVBP and AVTP are coupled together via the CWIPI library [61] to ensure the continuity of temperature and heat flux at the gas/solid boundary A_{gs}. More details and validation of the coupling method can be found in [62]. Conjugate heat transfer is necessary to retrieve the influence of unburnt gas preheating on the stabilization of the flame [10, 34, 54]. To reach steady-states until flashback occurs, an asynchronous coupling strategy between AVBP and AVTP similar to the one presented in [63] is used. The two codes can be de-synchronized in time, meaning that between two coupling iterations, as the slow thermal diffusion dominates the solid temperature, the time advancement in the solid is much faster than that in the fluid. This methodology was broadly tested and validated on a complex turbine blade configuration [64].

2.2. Configurations

The configuration is presented in Fig. 1, where a methane flame is stabilized over an asymmetrical pattern of slits. The 2D computational domain consists of a single periodical pattern, delimited by dashed lines, where a symmetry boundary condition is applied. The stream-wise direction is denoted x and the origin of x-axis and y-axis is the outer corner of the solid at the outlet of the main slit, represented by a grey disk in Fig. 1. The main geometrical parameters are the half-width D of the main slit, the half-width d of the auxiliary slit, the width W of the flame-holder (slit spacing) and its thickness e. Unless explicitly mentioned, the main slit half-width is fixed to $D = 0.5\,\mathrm{mm}$, the slit spacing to $W = 0.5\,\mathrm{mm}$, and the flame-holder thickness to $e = 1.0\,\mathrm{mm}$ in the following simulations. This represents the *baseline geometry*, for which the impact of the auxiliary slit half-width d is investigated by varying its half-width from $d = 0$ to $d = D$. Geometries presenting slit spacing and plate thickness different from the baseline case will however be studied in Section 5.4.
In the following, half-widths d and D may be quoted as widths to simplify the reading. The two slits are also referred to as

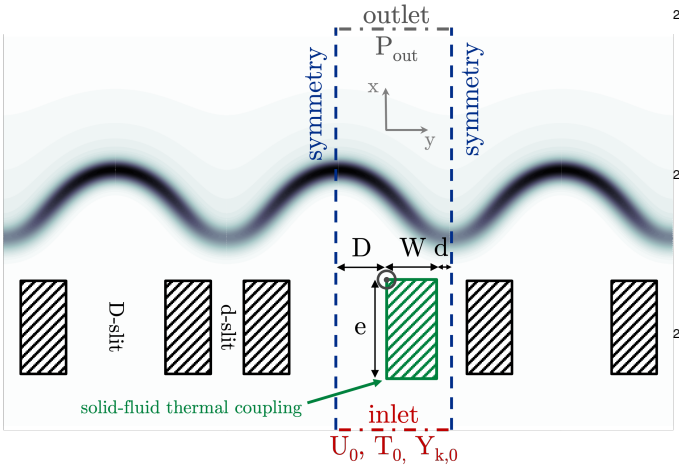

Figure 1: Numerical simulation domain with the main geometrical parameters and boundary conditions. The origin of x and y axes is indicated with the grey circle.

d-slit and *D-slit*, and flames on top of these slits as *d-flame* and *D-flame* for brevity. The total length of the numerical domain is $13(D+W)$ along the axial direction. The cases $d = 0$ and $d = D$ both represent symmetrical configurations with a different slit spacing, the flame-holder width of case $d = 0$ being twice larger ($2W$) than for $d = D$ where the solid width is W, as two solids are in contact through the boundary for $y = W$.

The boundary conditions at the inlet and the outlet are treated via the NSCBC formalism (Navier-Stokes Characteristic Boundary Conditions) [65]. The velocity U_0, temperature $T_u = 300\,\mathrm{K}$ and mixture composition $Y_{k,0}$ are imposed at the inlet, while a constant pressure $P_{out} = 1$ atm is imposed at the outlet. No-slip conditions and thermal coupling are imposed at the walls. The lateral sides of the fluid domain are treated as symmetries. The thermo-physical properties of the solid are taken from stainless steel with a density $\rho_s = 7869\,\mathrm{kg\,m^{-3}}$, a thermal capacity $c_s = 461\,\mathrm{J\,kg^{-1}\,K^{-1}}$, and a constant thermal conductivity $\lambda_s = 33\,\mathrm{W\,m^{-1}\,K^{-1}}$.

The characteristic size of mesh cells is 20 µm in the solid, 20 µm in the fluid close to the wall and 40 µm at both inlet and outlet. It has been checked that there are at least 15 points in the flame front for the thinnest (H2/air) flame investigated. Convergence in terms of mesh size has been verified by testing a mesh with half the cell size. For the most sensitive case ($d/D = 0.1$), the discrepancy was found limited to 0.4% for mass flow rates distribution, below 0.8% for local velocities and smaller than 0.6% for local heat release rate, with no impact on flame stabilization or flashback occurrence.

2.3. Procedure

The lean blow-off limit and flashback limit are investigated using the following protocol, which is repeated for a set of configurations with increasing auxiliary slit size d. For a given geometry, a flame is stabilized at an arbitrary mass flow rate inside the flame stability domain corresponding to some inlet flow velocity U_0. To determine the blow-off limit, the inlet velocity is incrementally increased, in small steps of $\Delta U = 0.02\,\mathrm{m\,s^{-1}}$ for methane and $\Delta U = 0.25\,\mathrm{m\,s^{-1}}$ for hydrogen, which leads in both cases to an uncertainty of about 5% on the limit. AVBP and AVTP are both unsteady solvers, but the calculations are carried out until a thermal equilibrium is reached in the gas and the solid. Following this procedure, the highest mass flow rate at which a simulation leads to a stabilized flame is considered to be the blow-off limit. Flashback is investigated in a similar way, where the inlet mass flow rate is instead incrementally decreased. The flashback limit is defined as the smallest mass flow rate for which a flame stabilizes above the flame-holder.

2.4. Influence of porosity

The overall burner porosity $\varepsilon = (D+d)/(D+d+W)$ varies with the auxiliary slit width d, which makes the interpretation of the results at fixed inlet velocity U_0 less intuitive, because of the associated variations in volumetric flow rate within the slits. It is thus convenient to introduce:

$$U_\varepsilon = U_0/\varepsilon \tag{1}$$

which represents the mean bulk velocity in the slits. Accordingly, the limits of blow-off and flashback will be plotted in the following as a function of $U_0/(\varepsilon S_L^0) = U_\varepsilon/S_L^0$. This representation enables comparisons at constant U_ε which corresponds to a kinematic equilibrium between the flame displacement speed and the bulk velocity in the slits.

2.5. Thermo-diffusive instabilities

In this study, as well as in previous symmetrical configurations [34, 53, 63], no Thermodiffusive Instabilities (TDI) have been observed. As shown by Matalon et al. [66] for close-to-unity Lewis number mixtures, TDI are damped for small disturbances wavelengths, i. e. large dimensionless wavenumbers $\kappa = k\delta_T$, where δ_T denotes the flame thickness. Sivashinsky [67] drew similar conclusions for non-unity Lewis numbers and small thermal expansion ratios. More recently, Berger et al. [68] determined the growth rate of TDI for H_2-air mixtures numerically without any assumption on the mixture Lewis number and on the thermal expansion ratio. They report negative growth rates for TDI beyond $\kappa \gtrsim 2.5$, with the exact instability threshold slightly varying with equivalence ratio. This dimensionless wavenumber corresponds to a wavelength between two and three times the flame thickness δ_T indicating that, in the small-scale configurations investigated in this study, TDI are damped and cannot develop. Preferential diffusion effects do manifest by creating locally enriched regions downstream of the flame-holder, but they do not result in any kind of time-evolving instability.

3. Wall flux analysis

Figure 2 presents a typical distribution of the heat release rate for a methane flame, together with streamlines in grey. This case is for methane at flashback limit for the baseline geometry defined in Section 2.2, with $d = 0.25$ mm. An auxiliary weak flame is visible on the right and is well separated from the main flame on the left. The rectangle in the middle represents the flame-holder where the heat flux density vectors $\mathbf{q} = \lambda_s \nabla T$, colored by their magnitude, are plotted. This vector field shows how heat from the combustion is redistributed to upstream reactants through the solid. A method to separate the contribution of each flame to the heating of reactants in each slits is now presented.

An energy balance is carried out by splitting the heat fluxes received and lost by the solid flame-holder as follows:

- On the upper left of the flame-holder, heat flux is received from D-flame: $\Phi_{\ulcorner} > 0$
- On the upper right of the flame-holder, heat flux is received from d-flame: $\Phi_{\urcorner} > 0$
- On the bottom left of the flame-holder, heat flux is lost to the fresh gases that are feeding the D-flame: $\Phi_{\llcorner} < 0$
- On the bottom right of the flame-holder, heat flux is lost to the fresh gases that are feeding the d-flame: $\Phi_{\lrcorner} < 0$

The separation between $\Phi_{\ulcorner}$ and $\Phi_{\urcorner}$ (respectively $\Phi_{\llcorner}$ and $\Phi_{\lrcorner}$) is denoted y_s and corresponds to a stagnation point. In some cases, stable recirculation zones appear downstream of the wall, requiring a more complex determination of y_s, which is detailed in the supplementary material. However, vortical structures periodically detaching from the flame holder and being convected downstream are not witnessed. Similarly, autoignition of fresh gases in the vicinity of the upstream wall is never observed in the studied configurations [54]. This is explained by the short residence time of reactants below the hot wall $\tau_r \sim W/U_b \sim 0.1$ ms for hydrogen flames near flashback, which remains small compared to the autoignition delay $\tau_i \sim 2$ s at the maximum temperature $T_w = 800$ K reached by the walls in present configurations.

Figure 2 illustrates that all the heat flux received through $\Phi_{\ulcorner}$ preheats the fresh gases through $\Phi_{\llcorner}$. However, a significant proportion of the flux received through $\Phi_{\urcorner}$ also exits through $\Phi_{\llcorner}$. This means that while the D-flame only preheats the flow entering the D-slit, the d-flame preheats both slits. This observation remains valid for all methane asymmetrical cases investigated. The consequences of this heat redistribution will be discussed in Sec. 4 for the methane flames. With hydrogen, this heat redistribution is however altered as will be discussed in Sec. 5.

In an effort to focus the analysis on physical mechanisms, the analysis concentrates on the worst-case scenarios for the operability limits associated to pure hydrogen for flashback resistance and pure methane for blow-off resistance. Intermediate fuel blends are anticipated to behave within these limit cases and are not explicitly examined in this study.

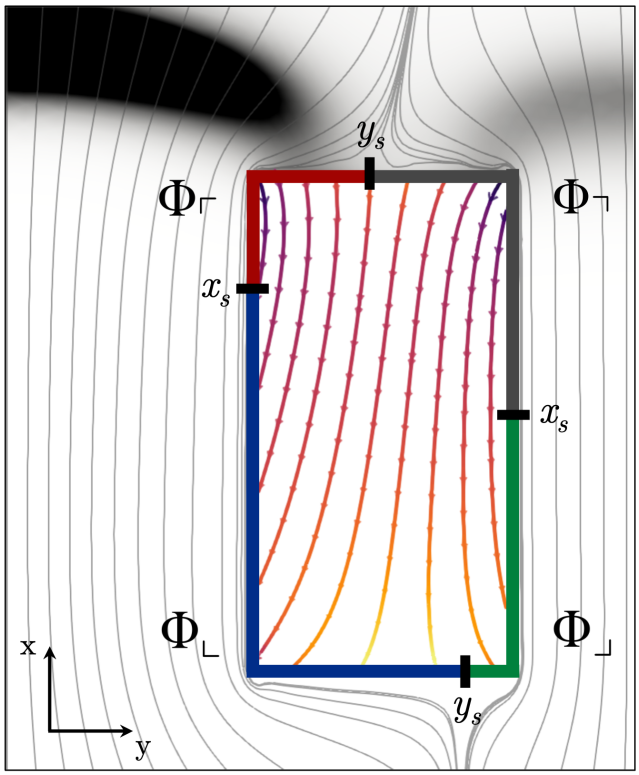

Figure 2: Heat flux distribution around the flame-holder for a methane flame at flashback limit, $D = 0.5$ mm, $W = 0.5$ mm, $d = 0.25$ mm, $e = 1$ mm. Background presents heat release rate and streamlines. Arrow lines in the solid correspond to heat flux density vectors which are colored by their magnitude (the highest being the darkest).

4. Lean blow-off limit of methane flames

The influence of auxiliary slit width d is now investigated for methane flames, with a focus on blow-off mechanism. Figure 3-(a) shows how the burner operability for methane changes when the ratio d/D is varied. Results are plotted versus U_e/S_L^0. For interpretation, note that larger (resp. lower) limit values for blow-off (resp. flashback) indicate extended burner operability. A first remark can be made about the two symmetrical cases, for which $d = 0$ shows a larger blow-off limit than $d = D$. This is consistent with the results from [10] for symmetrical flames. The larger slit spacing obtained with $d = 0$ increases the flame surface and the heat losses to the wall, improving flame anchoring.

As flashback is not critical for operation with methane, it is not further examined than the flashback limits presented in Fig. 3-(a). The most significant variations are changes of the blow-off limit with a marked extension near $d/D = 0.3$ and then a reduction. This observation confirms that compared to symmetrical configurations, auxiliary slits can efficiently delay blow-off of methane flames if their size is adequately

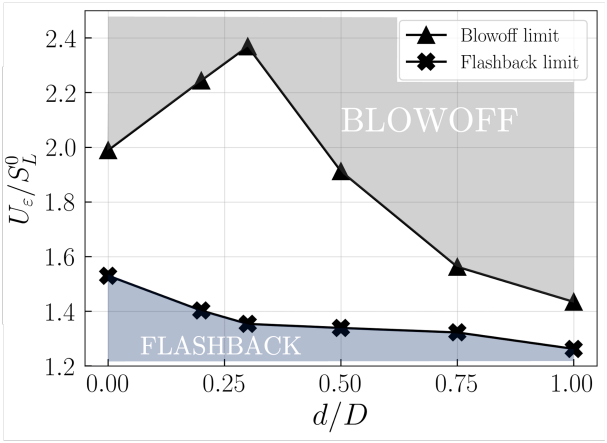

(a) Methane operability limits

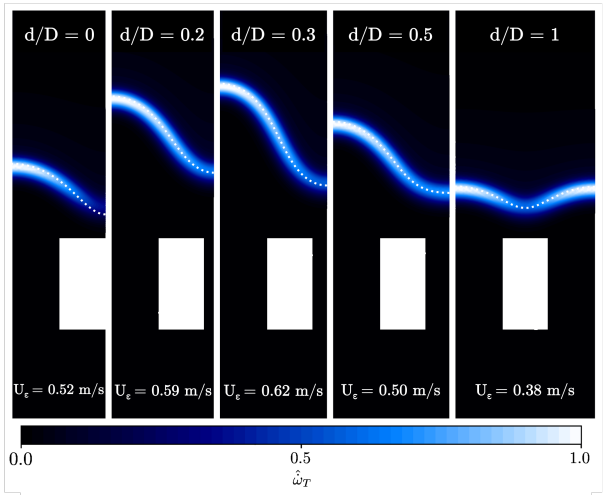

(b) Heat release rate at blow-off limit

Figure 3: (a) Operability map for methane flames as a function of d/D. (b) Heat release rate at blow-off limit, normalized by the maximum value $\dot{\omega}_{T,m} = 3\,\mathrm{GW\,m^{-3}}$. Dotted line is iso-$Y_{O_2} = 0.085$.

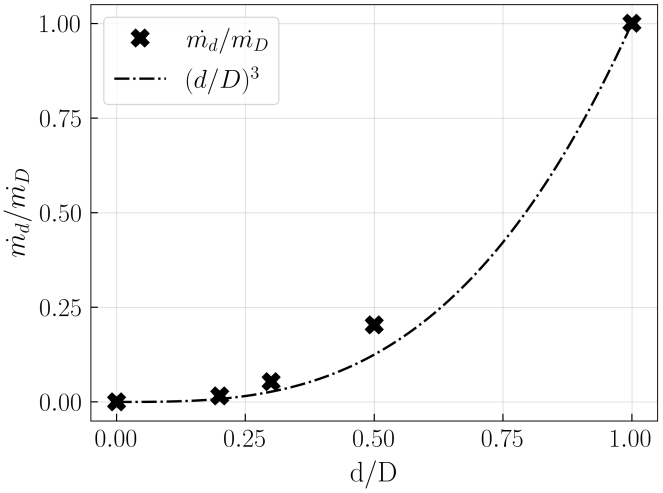

(a) Ratio of mass flow rates at blow-off limit

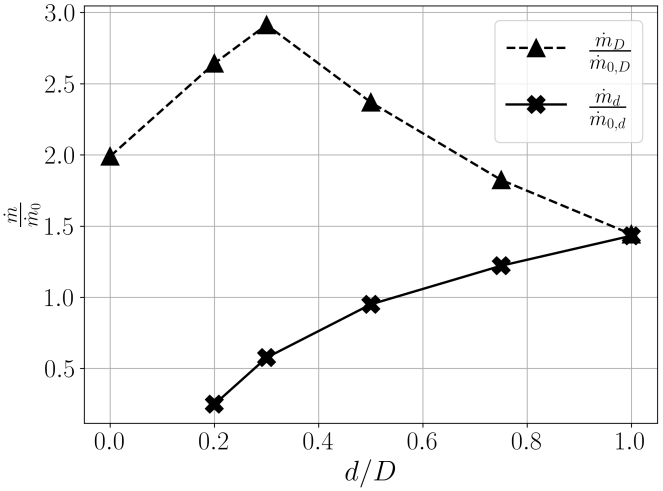

(b) Heat release rate at blow-off limit

Figure 4: (a) Ratio of mass flow rates in d-slit and D-slit at blow-off as a function of d/D. (b) Mass flow rate in each slit at blow-off limit normalized by the mass flow rate $\dot{m}_{0,d} = \rho_0 S_L^0 d$ from a 1D adiabatic flame over the same slit width.

selected. The governing mechanisms are scrutinized below by first examining the flame shapes.

4.1. Flame shape

Flames at lean blow-off limit are shown in Fig. 3-(b) by plotting the field of normalized heat-release rate, $\hat{\omega}_T$.

Notably, while for $d = D$ there are two bell-shaped flames above the slits, intermediate configurations and especially those of larger blow-off limit $d/D < 0.5$ do not show any detached, individual bell-shaped flame above the auxiliary slit. In these cases, the system behaves as a *single flame* whose feet are stabilized by the combustion due to the flow from the auxiliary slit. When the auxiliary slit width d is too close to the main hole width D ($d/D > 0.5$), a distinct flame is created above the auxiliary slit with a lower resistance to blow-off. The analysis now proceeds on a quantitative basis by examining how the mass flow rate, the heat release rate and the heat exchange is altered through each slits when the width d is varied.

4.2. Distribution of the mass flow rate

The relative proportions of mass flow rate passing through the two slits $\dot{m}_d$ and $\dot{m}_D$ is plotted Fig. 4-(a). Numerical results are also compared to predictions assuming a Hagen-Poiseuille velocity distribution [69] with constant thermo-physical properties in the two channels:

$$\dot{m}_d \sim G\frac{d^3}{12\nu} \qquad \text{and} \qquad \dot{m}_D \sim G\frac{D^3}{12\nu} \tag{2}$$

where the kinematic viscosity ν and the pressure gradient G are assumed to be roughly the same in the two slits. In this latter case, one is left with:

$$\frac{\dot{m}_d}{\dot{m}_D} \sim \left(\frac{d}{D}\right)^3 \tag{3}$$

Figure 4-(a) shows that the simulations are close to these predictions, indicating that a very limited mass flow rate flows through the auxiliary slit for small values of d/D. The impact on heat losses to the wall of these viscous effects is now detailed.

4.3. Sub-adiabatic combustion

Figure 3-(b) shows that the limited mass flow rates in small auxiliary slits are associated with flames stabilizing much closer to the solid than D-flames, promoting heat loss hence sub-adiabatic combustion. This effect can be quantified by normalizing the mass flow rate in each slit by that of a one-dimensional adiabatic flame that would pass through the slit:

$$\frac{\dot{m}_d}{\rho_0 S_L^0 d} = \frac{\dot{m}_d}{\dot{m}_{0,d}} \qquad \text{and} \qquad \frac{\dot{m}_D}{\rho_0 S_L^0 D} = \frac{\dot{m}_D}{\dot{m}_{0,D}} \tag{4}$$

where ρ_0 denotes the density of the inlet mixture. These ratios at blow-off limit are plotted in Fig. 4-(b). Deviations from unity may result from changes of the flame curvature, surface area and heat losses to the burner. Since any increase of the flame surface area or curvature leads to ratios equal to or above unity, any value below unity necessarily indicates a sub-adiabatic combustion.

Figure 4-(b) shows that an auxiliary slit with $0 < d/D < 0.7$ allows the flame in the main slit to resist to a larger ratio $\dot{m}_D/\dot{m}_{0,D}$ (*i.e.* a larger surface area and stretch) before being blown off than the symmetric configuration with $d/D = 0$. The peak of $\dot{m}_D/\dot{m}_{0,D}$ matches indeed exactly the peak of the blow-off limit in Fig. 3-(b).
In contrast, the ratio $\dot{m}_d/\dot{m}_{0,d}$ remains lower than unity for d-slit until $d/D \simeq 0.5$. As the d-flame is almost flat when d/D is small enough, the gap between $\dot{m}_d$ and $\dot{m}_{0,d}$ is directly correlated to d-flame heat losses to the flame-holder. This gap decreases as d/D increases and $\dot{m}_d/\dot{m}_{0,d} \simeq 1$ is reached for $d/D = 0.5$. Above $d/D = 0.5$, the d-slit flame is no longer sub-adiabatic and the ratio $\dot{m}_d/\dot{m}_{0,d}$ at blow-off increases as the flame bends. Concomitantly, resistance to blow-off worsens as d/D increases. Heat losses from the auxiliary flame to the burner therefore play a major role in the improvement of the blow-off limit of the overall system. The redistribution of these heat losses is now investigated.

4.4. Heat flux redistribution

The heat recirculated from the d-flame towards the fresh gases of the D-slit is determined in this section. To evaluate precisely the contribution of each flame in preheating each slit, the wall heat flux analysis presented in section 3 is now applied.

The (negative) fluxes received at the top of the flame-holder from each flame $\Phi_\ulcorner$ and $\Phi_\urcorner$ are balanced by the (positive) fluxes along the sides and the bottom of the flame-holder leading to a preheating of the fresh gases $\Phi_\llcorner$ and $\Phi_\lrcorner$according to the energy balance:

$$\Phi_\ulcorner + \Phi_\urcorner + \Phi_\llcorner + \Phi_\lrcorner = 0 \tag{5}$$

Though in general it is difficult to determine precisely from these four values where the heat received from each corner of the flame-holder is redistributed to the flow, the heat flux density vectors plotted in Fig. 2 clearly indicate that the D-slit is largely preheated by the heat received from the d-flame, whereas the D-flame only preheats the reactants in the D-slit. This has been checked for all methane asymmetrical cases explored in this study (not shown). In other words, it means that at blow-off, preheating of the fresh reactants is mostly driven by the auxiliary slit. Following that idea and noting that $|\Phi_\llcorner| > |\Phi_\ulcorner|$ always holds, the heat flux received by the D-slit from the d-flame can estimated as:

$$\Phi_{d\to D} = |\Phi_\llcorner| - |\Phi_\ulcorner| \tag{6}$$

which in turn can be expressed as a fraction of the total heat flux received by the D-slit:

$$\hat{\Phi}_{d\to D} = \Phi_{d\to D} / |\Phi_\llcorner| \tag{7}$$

a quantity which is plotted in Fig. 5 as a function of d/D. This figure shows that near the value $d/D = 0.3$, the fresh gases entering the D-slit are largely preheated by the d-flame, up to 60% of the total heat flux received by the D-slit. The strong similarities between Fig. 5 and Fig. 3-(a) confirm that asymmetrical auxiliary slits of intermediate size help to delay blow-off due to a redistribution of d-flame heat through the flame-holder to the reactants in the main slit.

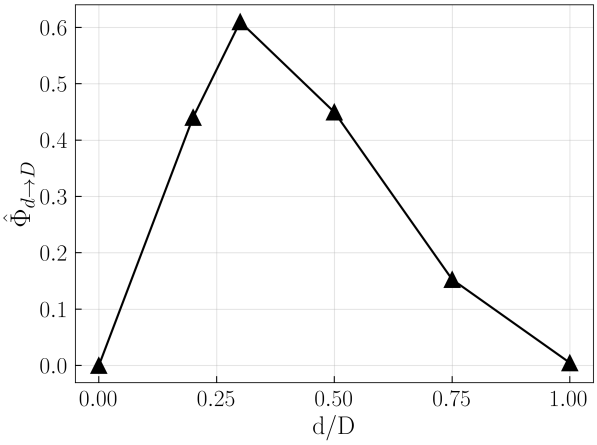

Figure 5: Share of preheat in D-slit received from d-flame for methane flames at the blow-off limit.

In summary, the impact of symmetry breaking on methane flame blow-off limits results from the following mechanisms:

- The mass flow rate in small auxiliary slits is limited by viscous losses and remains smaller than the mass flow rate of an adiabatic 1D flame.
- This causes the auxiliary d-flame to stabilize closer to the wall with a substantial heat transfer to the flame-holder that largely contributes to preheat the fresh gases within the main D-slit.
- This heat redistribution enables the flame in the main slit to handle a larger mass flow rate and a greater surface area before being blown off.

While the optimal configuration may vary under fully representative experimental conditions, similar hydrodynamic and thermal interactions are expected to take place in 3D laminar multi-perforated burners. This analysis elucidates the main mechanisms behind the enhancement of the blow-off limit for methane flames stabilized above asymmetrical geometries.

5. Flashback limits of hydrogen flames

The influence of slits symmetry breaking on hydrogen flames flashback is now investigated. The considered hydrogen-air flames are at an equivalence ratio $\Phi = 0.676$ to keep the same adiabatic temperature as the methane flames studied in the previous section. The conditions leading to blow-off are not discussed. Lean blow-off was found to take place at particularly high Reynolds numbers when the flow is turbulent. In addition, since hydrogen blow-off typically does not limit the operability of industrial burners, it is deemed out of scope.

Hydrogen flashback limits are plotted in Fig. 6-(a). The trend is clearly different from the methane flames shown in Fig. 3-(a), in which case U_ε/S_L^0 at flashback monotonously decreases for increasing d/D.
Here, two distinct extrema are found: one at $d/D = 0.2$ with a poor resistance to flashback and a second one at $d/D = 0.5$ with the highest resistance. The difference between the minimum and maximum hydrogen flashback limits exceeds 200% in Fig. 6-(a), while the maximum gap was about 25% for methane in Fig. 3-(a). The mechanisms responsible for these large differences are now investigated.

5.1. Flashback initiation

Figure 6-(b) shows the field of heat release rate of the hydrogen flames at the flashback limit when d/D is varied. The origin of flame upstream propagation during flashback is investigated.
Figures 7-(a) to (d) plot the position of the flame front foot ($Y_{O_2} = 0.19$ closest to the wall, highlighted in Fig. 6-(b)) for both d-flame and D-flame as a function of time. The symmetrical cases $d/D = 0$ and 1 feature identical initiation dynamics for d-flame and D-flame and are not presented for brevity. Two different initiations are observed: the d-flame triggers flashback for $d/D = 0.2$ and $d/D = 0.3$, whereas the D-flame propagates upstream first for larger auxiliary slit widths when $d/D = 0.5$ and $d/D = 0.75$. The d-slit flashback cases correspond to auxiliary widths $2d = 0.2$ mm and $2d = 0.3$ mm, as it is recalled that d corresponds to the half slit width. These widths can be compared to the quenching distance through a hole of the studied hydrogen flame at equivalence ratio $\Phi = 0.676$ and $T_u = T_0 = 300$ K, found to be $d_{Q,T_0} = 0.76$ mm in [70]. Observing flashback in slits much smaller than this quenching distance suggests that a huge preheat of the reactants occurs, as the quenching distance was found to decrease when preheat increases [71, 72, 73, 74]. This switch in flashback leading flame hints towards a competition between various physical mechanisms, and is somewhat counter-intuitive at first sight: why would auxiliary slits with a larger width d lead to preferential propagation through the D-slit?

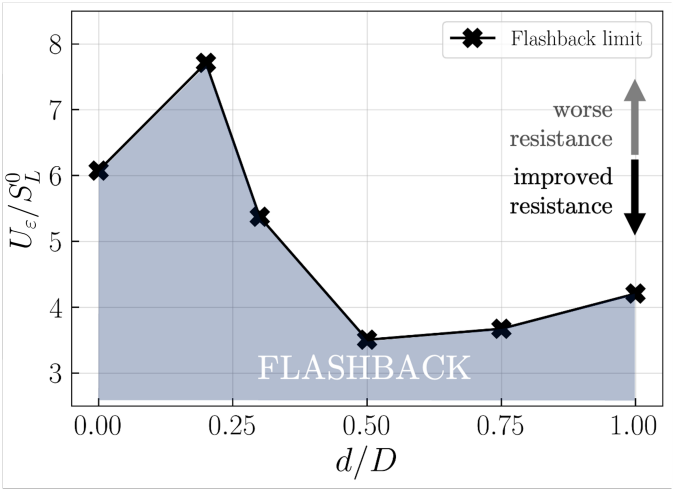

(a) Hydrogen flashback limit

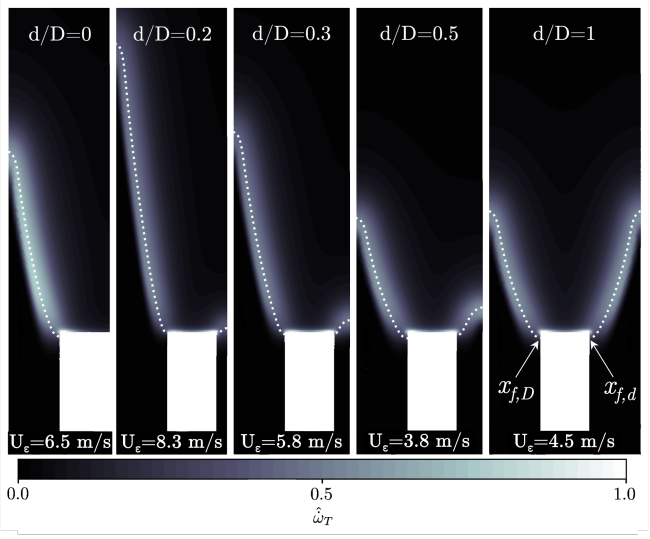

(b) Heat release rate at flashback limit

Figure 6: (a) Flashback limit of hydrogen flames as a function of d/D. (b) Heat release rate distribution of the hydrogen flames at flashback limit. Values are normalized by the maximum $\dot{\omega}_{T,m} = 19\,\mathrm{GW\,m^{-3}}$. Dotted line is iso-$Y_{O_2} = 0.19$.

5.2. d-slit flashback

One key point to understand why the flashback resistance worsens in Fig. 6-(a) for small auxiliary slits is to consider the competition between heat convection and heat diffusion through the d-slit. Figure 8-(a) displays the temperature fields at the flashback limit as a function of d/D, with the black line corresponding to the isoline of temperature $T = 600\,\mathrm{K}$. Figure 8-(b) shows the associated profiles in the d-slit at $x = -0.7$ mm, upstream of the reaction layer. To facilitate the reading, the abscissa in Fig. 8-(b) is an adapted normalized version of the y-coordinate $y'/d = (y - W)/d$, so that 0 corresponds to the d-side of the wall and 1 corresponds to the middle of the d-slit.

Figure 8 indicates that the preheat of the fresh gases in the

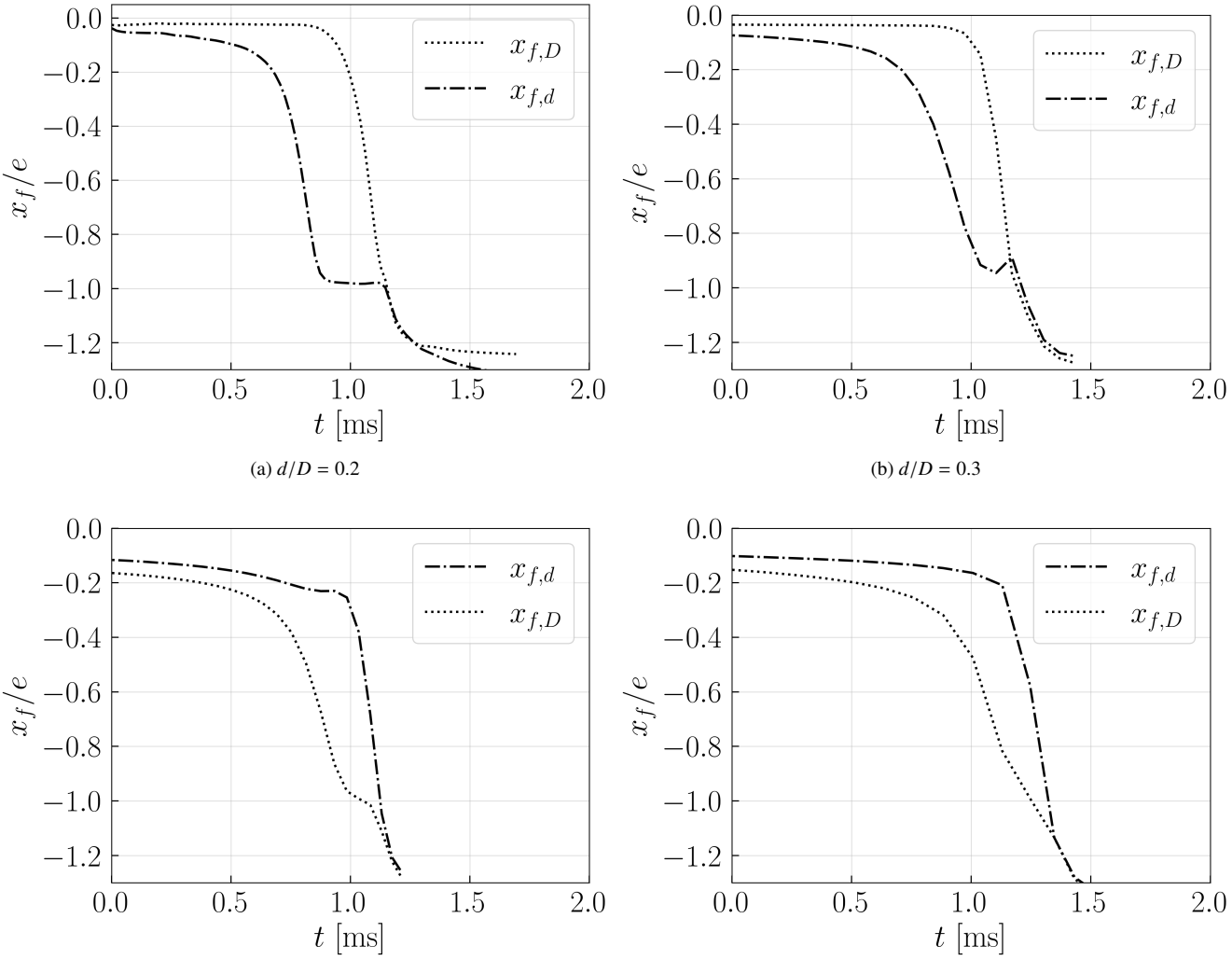

(a) $d/D = 0.2$ (b) $d/D = 0.3$

(c) $d/D = 0.5$ (d) $d/D = 0.75$

Figure 7: Position of the D-flame and d-flame tips at flashback initiation as a function of time, for $d/D = 0.2$, 0.3, 0.5 and 0.75.

auxiliary slit changes dramatically between $d/D = 0.2$ and $d/D = 0.5$. For small widths d, the reactants in the d-slit are preheated over the entire width of the slit, in which case heat transfer is dominated by thermal diffusion from the hot wall. Conversely, auxiliary slits with larger widths d are characterized by an increased penetration of the cold gases at $T_u = 300$ K inside the d-slit, in which cases heat convection in the center of the slit dominates thermal diffusion from the hot wall.

The competition between these two mechanisms can be estimated by assuming that a y-segment of gas advected through the d-slit is subjected to a 1D Fourier law $\partial T/\partial t = \alpha\,\partial^2 T/\partial y^2$ with a characteristic thermal diffusion time:

$$\tau_d = \frac{d^2}{\alpha} \tag{8}$$

where α is the thermal diffusivity of the gaseous mixture. The characteristic convection time is estimated as:

$$\tau_c = \frac{e}{U_\varepsilon} \tag{9}$$

where $U_\varepsilon = U_0/\varepsilon$ and e is the thickness of the flame-holder. A critical width, under which heat diffusion overcomes convection and penetrates the full extent of the slit width, can be defined as the width d_* for which the thermal diffusion time τ_d is equal to the characteristic convection time of gas τ_c inside the slit:

$$d_* \sim \left(\frac{\alpha e \varepsilon}{U_0}\right)^{1/2} \tag{10}$$

Evolution of d_* normalized by the main slit half width D is plotted in Fig. 9 as function of d/D. The thermal diffusivity is taken as the mean value in the reactants at the middle of the slit ($x = -0.5$ mm). The diagonal $x = y$ in Fig. 9 separates the domain into two regimes, the upper one dominated by heat diffusion, and the lower one dominated by convection.

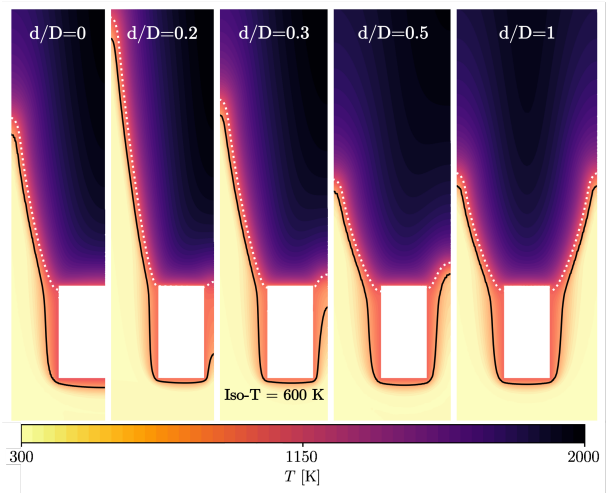

(a) Temperature distribution

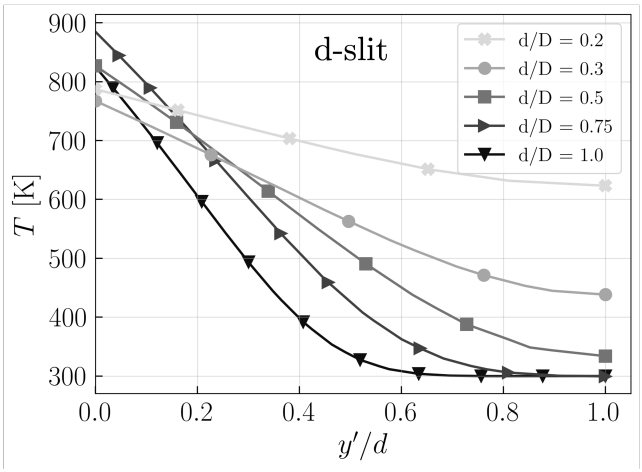

(b) Temperature profile at $x = -0.7$ mm

Figure 8: (a) Temperature distribution in the flowfield at flashback limit of hydrogen flames. White dotted line is the flame front. The black line is iso-$T = 600$ K. (b) Temperature profile in the d-slit at $x = -0.7$ mm, as a function of $y'/d = (y - W)/d$.

Figure 9 shows that the two cases with poor resistance to flashback $d/D = 0.2$ and $d/D = 0.3$ lie within or at the boundary of the heat-diffusion dominated domain. In these cases, the substantial preheating highlighted in Fig. 8 coupled to the high reactivity of hydrogen enable the d-flame to penetrate first within the slit, eventually leading to flashback.

Hence, to prevent penalizing the flashback limit, the width of the auxiliary d-slit must be greater than the critical thermal width d_*, thus avoiding excessive preheating of the reactants within the auxiliary slit, as shown by the temperatures at the center of the d-slit in Fig. 8-(b). The temperature of the gases at $x = -0.7$ mm and at the center of the d-slit remains almost equal to the inlet flow temperature $T_0 = 300$ K for $d/D \geq 0.5$. This corroborates observations from Fig. 9 that the auxiliary slit switched to a convection-dominated regime.

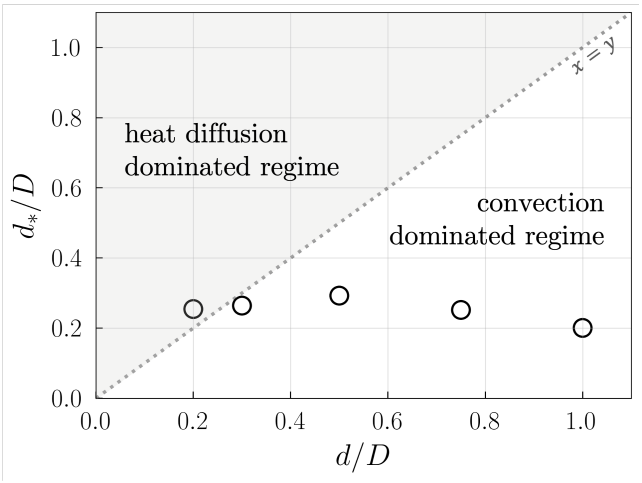

Figure 9: Critical widths d_* calculated at flashback limit using Eq. (10) for $d/D \neq 0$.

For $0.5 \leq d/D \leq 0.75$, corresponding to $0.5\,\text{mm} \leq 2d \leq 0.75\,\text{mm}$ in terms of slit width, the gases in the d-slit are barely preheated. The auxiliary slit is therefore small enough to quench the flame, given the previously mentioned quenching distance $d_{Q,T_0} = 0.76$ mm. This effect tends to disappear as d overcomes d_{Q,T_0}, partly explaining the degradation of the flashback resistance as d gets closer to D, which will now be detailed.

5.3. D-slit flashback

For large auxiliary d-slits $d/D = 0.5$ and $d/D = 0.75$, flashback is triggered in the main D-slit (see Figs. 7-(c-d)). The state of the flow within the main D-slit is now explored to understand this change of flashback regime.

Figure 10-(a) shows the velocity profiles at flashback limit at $x = -0.7$ mm. Results are normalized by the laminar burning velocity S_L^0 at $T_0 = 300$ K.

The first striking observation is that the velocity profiles in the main D-slit are almost superimposed for $d/D \geq 0.5$. All the more, Fig. 8-(b) shows that the temperature profile in the main slit remains unchanged as well from $d/D = 0.5$ to $d/D = 1$. The mass flow rate inside the main slit at flashback is therefore constant for flashback triggered by the main D-slit. This is in agreement with the standard flashback theory from Lewis and von Elbe [22, 38] based on the critical velocity gradient, endorsing the fact that when preheat becomes negligible, CVG remains applicable in the present cases.

Although flashback takes place with the same velocity profile in the main D-slit for $d/D \geq 0.5$, Fig. 10-(a) shows that velocity profiles in the auxiliary d-slit are different. Indeed, the velocity increases between $d/D = 0.5$ and $d/D = 1$, where it logically reaches the same profile as in the main slit. The reason behind these smaller velocities in the auxiliary slit is explained by Fig. 10-(b). It plots the evolution of the ratio of mass flow rates in each slit $\dot{m}_d/\dot{m}_D$. Results for an inviscid flow leading to a flat velocity distribution (d/D) and a Poiseuille velocity distribution calculated with Eq. (3) ($(d/D)^3$) are presented as

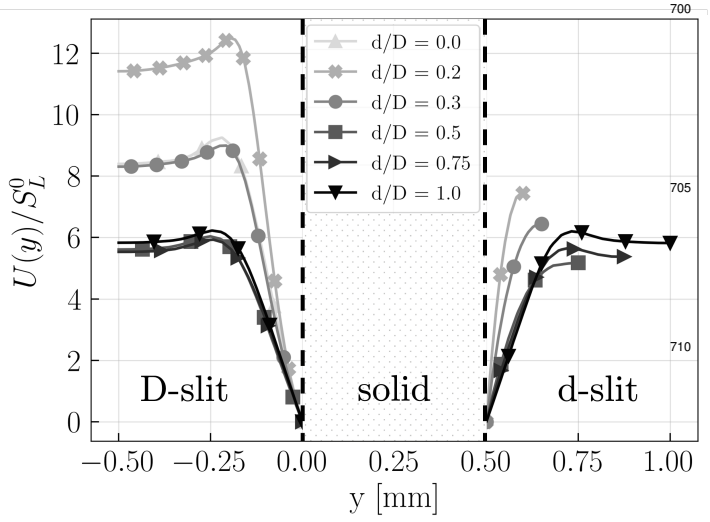

(a) Velocity profiles

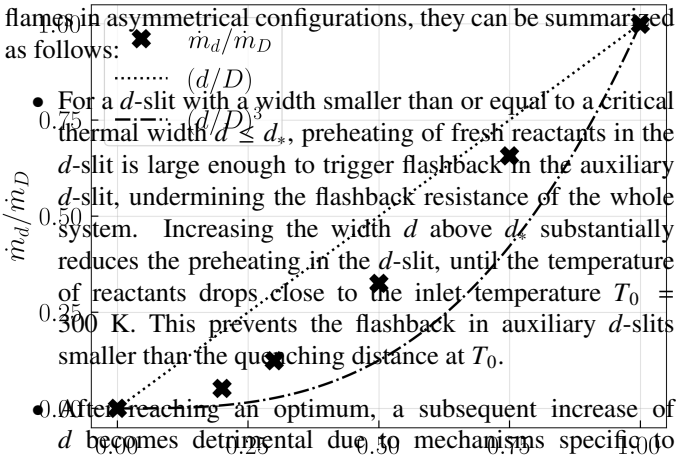

(b) Mass flow rates

Figure 10: (a) Velocity distribution at flashback limit at $x = -0.7$ mm. (b) Mass flow rates distribution in each slit compared to predictions from non-viscous (d/D) and viscous ($(d/D)^3$) models.

well. Deviation with respect to the Poiseuille distribution is further examined in supplementary material.

This figure confirms that, due to viscous losses, the mass flow rate $\dot{m}_d$ through the d-slit is smaller than the "share" of the total mass flow rate that would cross it for an ideal inviscid flow. In symmetrical cases $d = D$, bulk velocities in D-slit U_ε^D and in d-slit U_ε^d are the same $U_\varepsilon^D = U_\varepsilon^d = U_\varepsilon$. For asymmetrical cases $d < D$, Fig. 10-(b) shows that the mass flow rate $\dot{m}_d$ in d-slit is smaller than what would have been obtained for a flat velocity profile in both slits, meaning that $\dot{m}_d < \rho_u U_\varepsilon d$. The global mass balance indicates that:

$$\dot{m}_t = \dot{m}_D + \dot{m}_d = \rho_u U_\varepsilon^D D + \rho_u U_\varepsilon^d d \qquad (11)$$

where $\rho_u U_\varepsilon^d d < \rho_u U_\varepsilon d$. The mass flow rate $\dot{m}_D$ through the main slit therefore complies with $\rho_u U_\varepsilon^D D > \rho_u U_\varepsilon D$, leading to higher bulk velocities inside the main slit $U_\varepsilon^D > U_\varepsilon$.
This analysis corroborates that, if a given mass flow rate was to cross plates of the same porosity, a larger bulk velocity would be reached through the D-slit for asymmetrical configurations compared to symmetrical configurations. This explains the better resistance to flashback of the D-slit for $d/D = 0.5$ and $d/D = 0.75$ compared to the symmetrical cases $d/D = 0$ and $d/D = 1$ shown in Fig. 6-(a).

This increased resistance is also partly due to heat transfer from the main D-flame to the reactants in the d-slit, which is observed for $0.3 \leq d/D < 1$ and is not presented for brevity. This heat transfer goes in the opposite direction for hydrogen flames compared to methane flames. The d-slit therefore also acts as a thermal sink and further improves the D-slit flashback resistance.

Distinct mechanisms are found to drive flashback of hydrogen flames in asymmetrical configurations, they can be summarized as follows:

- For a d-slit with a width smaller than or equal to a critical thermal width $d \leq d_*$, preheating of fresh reactants in the d-slit is large enough to trigger flashback in the auxiliary d-slit, undermining the flashback resistance of the whole system. Increasing the width d above d_* substantially reduces the preheating in the d-slit, until the temperature of reactants drops close to the inlet temperature $T_0 = 300$ K. This prevents the flashback in auxiliary d-slits smaller than the quenching distance at T_0.
- After reaching an optimum, a subsequent increase of d becomes detrimental due to mechanisms specific to asymmetrical configurations. Viscous effects, at a given power density, result in higher bulk velocity in the D-slit for asymmetrical cases compared to symmetrical cases, enhancing the flashback resistance. This effect is augmented by the heat transfer from the D-flame to the d-slit, contributing to a further reduction of reactants preheating in the D-slit. These effects diminish as d approaches the value of D, leading to a decrease in flashback resistance.

The interplay of mechanisms related to symmetry breaking is observed to enhance the burner's resistance to flashback for hydrogen flames. To broaden the scope of this finding, additional configurations involving variations in slit spacing and wall thickness are explored.

5.4. Effect of wall thickness and slit spacing on hydrogen flashback

Modifications to the baseline geometry of the flame-holder are now considered and their impact on the flashback limit of hydrogen flames is examined. Results for the reference case with $W = 0.50$ mm and $e = 1.0$ mm are compared with simulations carried out for a flame-holder with a reduced width $W' = 0.25$ mm and for a flame-holder with a reduced thickness $e' = 0.5$ mm, all other parameters remaining unchanged. Results for U_ε/S_L^0 at flashback limit are plotted in Fig. 11-(a). The peak of U_ε/S_L^0 observed at $d/D = 0.2$ in Fig. 11-(a) is unchanged when the slit spacing is reduced from $W = 0.50$ mm to $W' = 0.25$ mm. However, this is not the case when the flame-holder thickness is reduced to $e' = 0.5$ mm. Indeed, the critical thermal width d_* in Eq. (10) scales as the square root of the wall thickness. Switching from a flame-holder with a thickness $e = 1$ mm to $e' = 0.5$ mm therefore reduces d_* by a factor 1.4. The impact of the flame-holder geometry on d_* is displayed in Fig. 11-(b). For a thinner flame-holder with a thickness $e' = 0.5$ mm, the critical thermal width drops to $d_*/D = 0.17$. This shift of the limit between the heat diffusion-dominated regime and the convection-dominated regime explains the absence of peak at $d/D = 0.20$ in Fig. 11-(a) for the thinner plate. To verify that the critical width remains a valid criterion, a supplementary condition at $d/D = 0.15$ is studied for $e' = 0.5$ mm. It is found to be particularly poorly resistant to

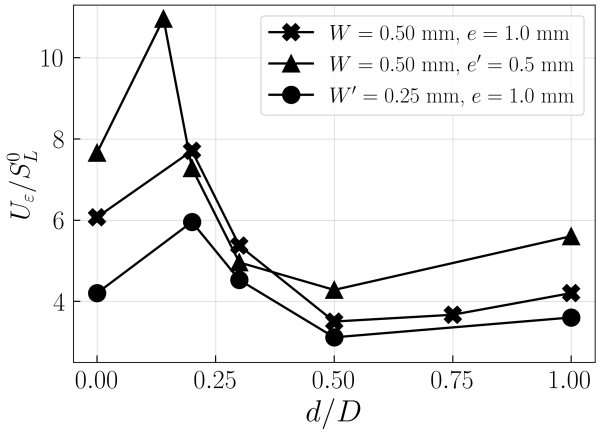

(a) Flashback limit

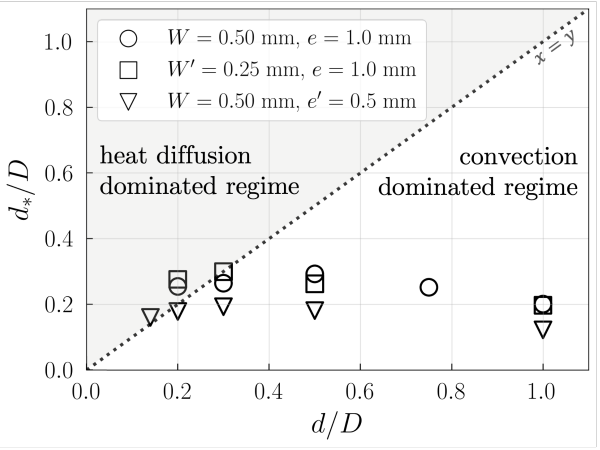

(b) Critical thermal width

Figure 11: Impact of the flame-holder geometry for hydrogen flames on (a) flashback limit U_ε/S_L^0 and (b) critical thermal width d_* deduced from Eq. (10).

flashback, similarly to cases at $d/D = 0.20$ for a larger plate thickness. It proves that the heat diffusion-dominated regime still exists and its limit is only shifted to $d_*/D = 0.17$.

This parametric analysis confirms that the global trend of the flashback limit remains unchanged when the geometry of the flame-holder is modified, the lowest resistance to flashback being only shifted as the critical width d_* varies. These additional results validate the mechanisms described earlier as the crucial phenomena for hydrogen flame flashback resistance in asymmetrical multi-perforated plates.

6. Conclusion

The impact of symmetry breaking on mechanisms limiting the stabilization of methane/air and hydrogen-air flames above asymmetrical slits has been investigated with two-dimensional direct numerical simulations.

Methane blow-off limits and hydrogen flashback limits have been examined by varying the width of the auxiliary d-slit relative to the width of the main D-slit. Results have been presented for mixtures with identical adiabatic flame temperatures, aligning with a standard operating point for numerous industrial laminar burners. A wall heat flux analysis that distinguishes the heat received by the flame-holder from each flame and its redistribution to the reactants in each slit has been used to interpret the results.

Mechanisms leading to an improved blow-off resistance of methane flames stabilized above asymmetrical slits have been unveiled. For sufficiently small auxiliary d-slits, viscous dissipation limits the mass flow rate in the d-slit which remains smaller than the mass flow rate of an adiabatic freely propagating one-dimensional flame. This asymmetry generates a heat redistribution from the d-flame to the reactants flowing in the main D-slit, leading to a more robust flame that can then sustain a larger mass flow rate, higher stretch and greater surface area before being blown off.

The flashback of hydrogen flames has been observed to be highly sensitive to the asymmetry of the slits. Various mechanisms with opposing effects have been identified, leading to a non-monotonic behavior. For auxiliary slits smaller than a critical thermal width, the flashback resistance has been found to be impaired by the important preheat of fresh gases in d-slit, leading to flashback initiation in the small auxiliary slit. Increasing d improves the flashback limit up to a factor two, as the preheat of fresh gases in d-slit decreases. It reaches a point where the preheat becomes too weak to trigger flashback in d-slit. The flashback is then only driven by the critical velocity gradient in the main D-slit, which is wider than the quenching distance of the studied flame at T_0. In these cases, viscous dissipation in the small d-slit increases the bulk velocity in the larger D-slit, improving its flashback resistance. Additionally, the small d-slit becomes a thermal sink for the main slit. Quenching, as well as viscous and thermal dissipation in the small d-slit progressively weaken as the configuration approaches symmetry, reducing flashback resistance.
The interplay of these mechanisms gives rise to the existence of an asymmetrical configuration where flashback resistance is enhanced compared to symmetrical cases. This counter-intuitive result, identified for the first time, has been validated across different burner thicknesses and slit spacings. It underscores the significance of asymmetrical configurations in the design of fuel-flexible multi-perforated burners, influencing both ends of the operating range, *i.e.* the lean blow-off of methane flames and the flashback of hydrogen flames.

7. Acknowledgments

We acknowledge the support received from the SERMETA Research and Development Laboratory. We also acknowledge the funding received from the Association Nationale Recherche Technologie (ANRT) through the CIFRE grant n° 2021/1069.
This project has received funding from the European Union's HORIZON 2020, European Research Council (ERC), Grant agreement 832248 SCIROCCO.
This work was granted access to the HPC resources of IDRIS under the allocation 2023-A0132B10627 made by GENCI.

References

[1] S. Griffiths, B. K. Sovacool, J. Kim, M. Bazilian, J. M. Uratani, Industrial decarbonization via hydrogen: A critical and systematic review of developments, socio-technical systems and policy options, Energy Res Soc Sci 80 (2021) 102208.

[2] T. Capurso, M. Stefanizzi, M. Torresi, S. Camporeale, Perspective of the role of hydrogen in the 21st century energy transition, Energ Convers Manage 251 (2022) 114898.

[3] G. Gahleitner, Hydrogen from renewable electricity: An international review of power-to-gas pilot plants for stationary applications, Int J Hydrogen Energy 38 (2013) 2039–2061.

[4] H. Blanco, A. Faaij, A review at the role of storage in energy systems with a focus on power to gas and long-term storage, Renew Sust Energ Rev 81 (2018) 1049–1086.

[5] F. Halter, C. Chauveau, I. Gökalp, Characterization of the effects of hydrogen addition in premixed methane/air flames, Int J Hydrogen Energy 32 (2007) 2585–2592.

[6] H. de Vries, A. V. Mokhov, H. B. Levinsky, The impact of natural gas/hydrogen mixtures on the performance of end-use equipment: Interchangeability analysis for domestic appliances, Appl Energ 208 (2017) 1007–1019.

[7] D. R. Jones, W. A. Al-Masry, C. W. Dunnill, Hydrogen-enriched natural gas as a domestic fuel: an analysis based on flash-back and blow-off limits for domestic natural gas appliances within the uk, Sustain Energy Fuels 2 (2018) 710–723.

[8] H. de Vries, H. B. Levinsky, Flashback, burning velocities and hydrogen admixture: Domestic appliance approval, gas regulation and appliance development, Appl Energ 259 (2020) 114116.

[9] M. Fukuda, K. Korematsu, M. Sakamoto, On quenching distance of mixtures of methane and hydrogen with air., Bull. JSME 24 (1981) 1192–1197.

[10] H. M. Altay, K. S. Kedia, R. L. Speth, A. F. Ghoniem, Two-dimensional simulations of steady perforated-plate stabilized premixed flames, Combust Theory Model 14 (2010) 125–154.

[11] A. Aniello, T. Poinsot, L. Selle, T. Schuller, Hydrogen substitution of natural-gas in premixed burners and implications for blow-off and flashback limits, Int J Hydrogen Energy 47 (2022) 33067–33081.

[12] T. B. Kıymaz, E. Böncü, D. Güleryüz, M. Karaca, B. Yılmaz, C. Allouis, İskender Gökalp, Numerical investigations on flashback dynamics of premixed methane-hydrogen-air laminar flames, Int J Hydrogen Energy 47 (2022) 25022–25033.

[13] M. W. Melaina, O. Antonia, M. Penev, Blending hydrogen into natural gas pipeline networks: a review of key issues, Report No. NREL/TP-5600 – 51995, Office of Scientific and Technical Information, U.S. Department of Energy, Oak Ridge, TN, USA, 2013.

[14] Y. J. Kim, B. J. Lee, H. G. Im, Hydrodynamic and chemical scaling for blow-off dynamics of lean premixed flames stabilized on a meso-scale bluff-body, Proc. Combust. Inst. 37 (2019) 1831–1841.

[15] J. Wan, H. Zhao, Blow-off mechanism of a holder-stabilized laminar premixed flame in a preheated mesoscale combustor, Combust Flame 220 (2020) 358–367.

[16] R. Lamioni, C. Bronzoni, M. Folli, L. Tognotti, C. Galletti, Feeding H_2-admixtures to domestic condensing boilers: Numerical simulations of combustion and pollutant formation in multi-hole burners, Appl Energ 309 (2022) 118379.

[17] K. Wohl, N. M. Kapp, C. Gazley, The stability of open flames, Symp. (Int.) Combust. 3 (1948) 3–21.

[18] K. S. Kedia, A. F. Ghoniem, Mechanisms of stabilization and blowoff of a premixed flame downstream of a heat-conducting perforated plate, Combust Flame 159 (2012) 1055–1069.

[19] F. H. Vance, Y. Shoshin, L. de Goey, J. A. van Oijen, An investigation into flashback and blow-off for premixed flames stabilized without a recirculation vortex, Combust Flame 235 (2022) 111690.

[20] A. M. Gamal, A. H. Ibrahim, E.-M. M. Ali, F. M. Elmahallawy, A. Abdelhafez, M. A. Nemitallah, S. S. Rashwan, M. A. Habib, Structure and lean extinction of premixed flames stabilized on conductive perforated plates, Energy Fuels 31 (2017) 1980–1992.

[21] C. K. Law, Combustion physics, Cambridge university press, 2010.

[22] B. Lewis, G. V. Elbe, Stability and structure of burner flames, J Chem Phys 11 (1943) 75–93.

[23] B. Lewis, G. Von Elbe, Combustion, flames and explosions of gases, Elsevier, 2012.

[24] B. Karlovitz, D. Denniston Jr, D. Knapschaefer, F. Wells, Studies on turbulent flames: A. flame propagation across velocity gradients b. turbulence measurement in flames, Symp. (Int.) Combust. 4 (1953) 613–620.

[25] A. Melvin, J. Moss, Evidence for the failure of the flame stretch concept for premixed flames, Combust Sci Technol 7 (1973) 189–196.

[26] T. Kawamura, K. Asato, T. Mazaki, T. Hamaguchi, H. Kayahara, Explanation of the blowoff of inverted flames by the area-increase concept, Combust Flame 35 (1979) 109–116.

[27] T. Kawamura, K. Asato, T. Mazaki, Reexamination of the blowoff mechanism of premixed flames—inverted flames, Combust Flame 45 (1982) 225–233.

[28] C. Trevino, F. Méndez, Asymptotic analysis of the ignition of hydrogen by a hot plate in a boundary layer flow, Combust Sci Technol 78 (1991) 197–216.

[29] C. Sung, C. Law, A. Umemura, On adiabatic stabilization of inverted flames, Symp. (Int.) Combust. 24 (1992) 205–212.

[30] S. J. Shanbhogue, S. Husain, T. Lieuwen, Lean blowoff of bluff body stabilized flames: Scaling and dynamics, Prog Energy Combust Sci 35 (2009) 98–120.

[31] J. Wan, A. Fan, H. Yao, W. Liu, Experimental investigation and numerical analysis on the blow-off limits of premixed CH_4/air flames in a mesoscale bluff-body combustor, Energy 113 (2016) 193–203.

[32] K. S. Kedia, A. F. Ghoniem, The blow-off mechanism of a bluff-body stabilized laminar premixed flame, Combust Flame 162 (2015) 1304–1315.

[33] A. Fan, J. Wan, Y. Liu, B. Pi, H. Yao, W. Liu, Effect of bluff body shape on the blow-off limit of hydrogen/air flame in a planar micro-combustor, Appl Therm Eng 62 (2014) 13–19.

[34] F. Vance, L. de Goey, J. van Oijen, Development of a flashback correlation for burner-stabilized hydrogen-air premixed flames, Combust Flame 243 (2022) 112045.

[35] F. H. Vance, Y. Shoshin, L. P. de Goey, J. A. van Oijen, Flame stabilization regimes for premixed flames anchored behind cylindrical flame holders, Proc. Combust. Inst. 38 (2021) 1983–1992.

[36] M. R. Johnson, L. W. Kostiuk, R. K. Cheng, A ring stabilizer for lean premixed turbulent flames, Combust Flame 114 (1998) 594–596.

[37] B. Bédat, R. K. Cheng, Effects of buoyancy on premixed flame stabilization, Combust Flame 107 (1996) 13–26.

[38] G. V. Elbe, M. Mentser, Further studies of the structure and stability of burner flames, J Chem Phys 13 (1945) 89–100.

[39] B. A. A. Putnam, R. A. Jensen, Application of dimensionless numbers to flash-back and other combustion phenomena, Symp. (Int.) Combust. 3 (1976) 89–98.

[40] A. Kalantari, V. McDonell, Boundary layer flashback of non-swirling premixed flames: Mechanisms, fundamental research, and recent advances, Prog Energy Combust Sci 61 (2017) 249–292.

[41] P. Kurz, Some factors influencing stability limits of bunsen flames, Combust Flame 1 (1957) 162–178.

[42] V. Kurdyumov, E. Fernandez-Tarrazo, J.-M. Truffaut, J. Quinard, A. Wangher, G. Searby, Experimental and numerical study of premixed flame flashback, Proc. Combust. Inst. 31 (2007) 1275–1282.

[43] J. Grumer, M. E. Harris, Temperature dependence of stability limits of burner flames, Ind Eng Chem 46 (1954) 2424–2430.

[44] G. L. Dugger, Flame stability of preheated propane-air mixtures, Ind Eng Chem 47 (1955) 109–114.

[45] M. Mizomoto, Y. Asaka, S. Ikai, C. Law, Effects of preferential diffusion on the burning intensity of curved flames, Symp. (Int.) Combust. 20 (1985) 1933–1939.

[46] F. H. Vance, P. de Goey, J. A. van Oijen, The effect of thermal diffusion on stabilization of premixed flames, Combust Flame 216 (2020) 45–57.

[47] V. Hoferichter, C. Hirsch, T. Sattelmayer, Prediction of confined flame flashback limits using boundary layer separation theory, J Eng Gas Turbines Power 139 (2017) 021505.

[48] V. Hoferichter, C. Hirsch, T. Sattelmayer, Analytic prediction of unconfined boundary layer flashback limits in premixed hydrogen–air flames, Combust Theory Model 21 (2017) 382–418.

[49] K. Aung, M. Hassan, G. Faeth, Effects of pressure and nitrogen dilution on flame/stretch interactions of laminar premixed $H_2/O_2/N_2$ flames,

Combust Flame 112 (1998) 1–15.
[50] F. Dabireau, B. Cuenot, O. Vermorel, T. Poinsot, Interaction of flames of $H_2 + O_2$ with inert walls, Combust Flame 135 (2003) 123–133.
[51] C. Jainski, M. Rißmann, B. Böhm, J. Janicka, A. Dreizler, Sidewall quenching of atmospheric laminar premixed flames studied by laser-based diagnostics, Combust Flame 183 (2017) 271–282.
[52] H. Kosaka, F. Zentgraf, A. Scholtissek, C. Hasse, A. Dreizler, Effect of flame-wall interaction on local heat release of methane and dme combustion in a side-wall quenching geometry, Flow Turbul Combust 104 (2020) 1029–1046.
[53] F. Fruzza, R. Lamioni, L. Tognotti, C. Galletti, Flashback of H_2-enriched premixed flames in perforated burners: Numerical prediction of critical velocity, Int J Hydrogen Energy (2023). doi:10.1016/j.ijhydene.2023.04.252.
[54] H. Pers, A. Aniello, F. Morisseau, T. Schuller, Autoignition-induced flashback in hydrogen-enriched laminar premixed burners, Int J Hydrogen Energy 48 (2023) 10235–10249.
[55] A. L. Sánchez, F. A. Williams, Recent advances in understanding of flammability characteristics of hydrogen, Prog Energy Combust Sci 41 (2014) 1–55.
[56] R. Lamioni, C. Bronzoni, M. Folli, L. Tognotti, C. Galletti, Effect of slit pattern on the structure of premixed flames issuing from perforated burners in domestic condensing boilers, Combust Theory Model 27 (2023) 218–243.
[57] Cerfacs avbp website, https://www.cerfacs.fr/avbp7x/, accessed: 2022-06-30.
[58] T. Schonfeld, M. Rudgyard, Steady and unsteady flow simulations using the hybrid flow solver avbp, AIAA journal 37 (1999) 1378–1385.
[59] V. Moureau, G. Lartigue, Y. Sommerer, C. Angelberger, O. Colin, T. Poinsot, Numerical methods for unsteady compressible multi-component reacting flows on fixed and moving grids, J Comput Phys 202 (2005) 710–736.
[60] P.-A. Masset, F. Duchaine, A. Pestre, L. Selle, Modelling challenges of volume-averaged combustion in inert porous media, Combust Flame 251 (2023) 112678.
[61] F. Duchaine, S. Jauré, D. Poitou, E. Quémerais, G. Staffelbach, T. Morel, L. Gicquel, Analysis of high performance conjugate heat transfer with the openpalm coupler, Comput Sci Discov 8 (2015) 015003.
[62] F. Duchaine, A. Corpron, L. Pons, V. Moureau, F. Nicoud, T. Poinsot, Development and assessment of a coupled strategy for conjugate heat transfer with large eddy simulation: application to a cooled turbine blade, Int J Heat Fluid Flow 30 (2009) 1129–1141.
[63] E. Flores-Montoya, A. Aniello, T. Schuller, L. Selle, Predicting flashback limits in H_2 enriched CH_4/air and C_3H_8/air laminar flames, Combust Flame 258 (2023) 113055.
[64] F. Duchaine, N. Maheu, V. Moureau, G. Balarac, S. Moreau, Large-eddy simulation and conjugate heat transfer around a low-mach turbine blade, J Turbomach Trans ASME 136 (2014) 051015.
[65] T. J. Poinsot, S. Lelef, Boundary conditions for direct simulations of compressible viscous flows, J Comput Phys 101 (1992) 104–129.
[66] M. Matalon, C. Cui, J. Bechtold, Hydrodynamic theory of premixed flames: effects of stoichiometry, variable transport coefficients and arbitrary reaction orders, J Fluid Mech 487 (2003) 179–210.
[67] G. Sivashinsky, Diffusional-thermal theory of cellular flames, Combust Sci Technol 15 (1977) 137–145.
[68] L. Berger, A. Attili, H. Pitsch, Intrinsic instabilities in premixed hydrogen flames: Parametric variation of pressure, equivalence ratio, and temperature. part 1 - dispersion relations in the linear regime, Combust Flame 240 (2022) 111935.
[69] H. Schlichting, J. Kestin, Boundary layer theory, Vol. 121, Springer, 1961.
[70] Y. Jung, M. J. Lee, N. I. Kim, Direct prediction of laminar burning velocity and quenching distance of hydrogen-air flames using an annular stepwise diverging tube (asdt), Combust Flame 164 (2016) 397–399.
[71] H. Kosaka, F. Zentgraf, A. Scholtissek, L. Bischoff, T. Häber, R. Suntz, B. Albert, C. Hasse, A. Dreizler, Wall heat fluxes and CO formation/oxidation during laminar and turbulent side-wall quenching of methane and DME flames, Int J Heat Fluid Flow 70 (2018) 181–192.
[72] C. Hasse, M. Bollig, N. Peters, H. Dwyer, Quenching of laminar iso-octane flames at cold walls, Combust Flame 122 (2000) 117–129.
[73] T. Zirwes, T. Häber, F. Zhang, H. Kosaka, A. Dreizler, M. Steinhausen, C. Hasse, A. Stagni, D. Trimis, R. Suntz, et al., Numerical study of quenching distances for side-wall quenching using detailed diffusion and chemistry, Flow Turbul Combust 106 (2021) 649–679.
[74] L. Xu, F. Yan, Y. Wang, Effects of hydrogen addition on the standoff distance of premixed burner-stabilized flames of various hydrocarbon fuels, Energy Fuels 32 (2018) 2385–2396.